Spectrochimica Acta Part B 74–75 (2012) 57–65

Contents lists available at SciVerse ScienceDirect

Spectrochimica Acta Part B

journal homepage: www.elsevier.com/locate/sab

Testing a portable laser-induced breakdown spectroscopy system on geological samples

Jozef Rakovský [a,b,*], Olivier Musset [a], JeanFrançois Buoncristiani [c], Vincent Bichet [d], Fabrice Monna [e], Pascal Neige [c], Pavel Veis [b,f]

[a] Laboratoire interdisciplinaire Carnot de Bourgogne, UMR 6303 CNRS, Université de Bourgogne, 9 Av. A. Savary, BP 47 870, F-21078 Dijon Cedex, France
[b] Department of Experimental Physics FMFI, Comenius University, Mlynská dolina, 842 48 Bratislava, Slovakia
[c] Laboratoire Biogéosciences, UMR CNRS 6282, Université de Bourgogne, 6 Boulevard Gabriel 21000 Dijon, France
[d] Laboratoire Chrono-Environnement, UMR CNRS 6249, Université de Besançon, 16 Route de Gray 25000 Besançon, France
[e] Laboratoire ARTéHIS, UMR CNRS 6298, Université de Bourgogne, 6 Boulevard Gabriel 21000 Dijon, France
[f] State Geological Institute of Dionýz Štúr, Mlynská dolina 1, 817 04 Bratislava 11, Slovakia

ARTICLE INFO

Article history:
Received 2 January 2012
Accepted 7 July 2012
Available online 20 July 2012

Keywords:
Portable LIBS
LIBS cartography
Tephra
Ammonite
Fossilization

ABSTRACT

This paper illustrates the potentialities of a home-made portable LIBS (laser-induced breakdown spectroscopy) instrument in Earth sciences, more particularly in geochemically recognizing (i) tephra layers in lacustrine sediments and (ii) fossilization processes in ammonites. Abundances for selected lines of Al, Ca, Fe, Ti, Ba and Na were determined in lacustrine chalk sediments of the Jura, where the Laacher See Tephra (LST) layer is recorded. A statistical treatment of elemental maps produced from the section of a sedimentary column containing the LST event allows instrumental conditions to be optimized. Accumulating spectra from close shot positions gives better results than multiplying shots at the same location. A depth profile method was applied to study ammonite fossilization (pyritization, phosphatization) processes. Depth variations of Fe, Ca, Al intensities, and Fe/Ca and Al/Ca ratios provide indications about pyritization, but phosphatization processes cannot be determined with our device.

1. Introduction

Many laser-induced breakdown spectrometry (LIBS) devices have already been developed, as the literature shows (Hahn et al., 2012 [1], and references cited therein). The simplicity of the apparatus creates a natural demand for a portable LIBS system with on-site measurement capabilities. The standard device consists of two main parts: a laser for plasma generation, and a spectrometer for spectral analyses of light from the plasma [2]. Cremers et al. (1996) presented a transportable device equipped with a long fiber which was able to deliver a laser pulse to a sample, and to collect light emitted from the plasma [3]. The same year, a compact suitcase system weighing 14.6 kg was presented for the first time [4]. This system was the basis for a new generation of instrument developed by Wainner et al. (2001) [5], finally used for geochemical analyses in 2005 [6]. A few commercial and portable LIBS systems are nowadays available on the market: Easy LIBS from IVEA© (which integrates the compact laser developed in our lab), PL100-GEO from Applied Spectra©, LIBSCAN 25 from Applied Photonics©, Porta-LIBS-2000 from StellarNet Inc.©, and IDEALIBS from Bertin Technologies©. Most of them are heavy (up to 25 kg) and transportable rather than portable. In the lightest systems, lasers are either very expensive to attain high performance with reduced volume or if costs are lower, performance is reduced.

In geosciences and archeology, portable LIBS instruments have already been used to identify alteration layers in speleothems, using depth profiles of Sr and Ca [7], for in-situ analysis of bronze artifacts according to their compositional classification [8], and for quarry identification of historical building material [9]. A light LIBS system (ChemCam), representing less than 10 kg of the total payload, has been implemented in the rover Curiosity, which is en route to the planet Mars, with an expected arrival time in August 2012. There are also many papers on the capabilities of such a system to obtain immediate results without sample preparation or use of chemical reagents [10,11].

In the present study, a portable LIBS was developed to make the instrument as small and light as possible. It consists of a small Nd:YAG laser developed in our laboratory [12], a small compact spectrometer, and a laptop computer. The control of the laser, the acquisition and analysis of the spectra are performed by lab-made software which can be directly operated by the computer touch screen. The aim is to assess its potential for Earth sciences as a tool for geologists in two circumstances: (i) to recognize volcanic eruption ash in sedimentary sequences (tephra layer) and (ii) to evaluate the fossilization processes of ammonites.

* Corresponding author at: Department of Experimental Physics FMFI, Comenius University, Mlynská dolina, 842 48 Bratislava, Slovakia.
E-mail address: jozef.rakovsky@fmph.uniba.sk (J. Rakovský).

0584-8547/$ – see front matter © 2012 Elsevier B.V. All rights reserved.
doi:10.1016/j.sab.2012.07.018

In event stratigraphy, volcanic eruptions and subsequent ash deposits are among the best chronostratigraphical markers. During the late Quaternary, the Eifel was the major volcanic complex in Germany. Two main tephra layers are related to this volcanic complex: the Ulmener Maar Tephra (UMT), and the Laacher See Tephra (LST), which produced the greatest geographical extension of ash fall. The age of the LST is 13,180 ± 40 calibrated years BP [13]. The eruption was multi-phased with 3 main ash falls [14,15]. Its occurrence is recorded in the Jura mountains, located about 500 km from the source, as mm-thick dark layers in lake sediments [16,17]. However, in the field, it is difficult to identify the origin of dark layers, which could either be LST or simply organic. In this case, the identification of tephra can be performed via the on-site measurement of magnetic susceptibility because ash particles are frequently more magnetic than the surrounding sediment, or possibly at the laboratory via geochemical measurements. Conventional geochemical analyses are often destructive and time-consuming because of sample preparation. That is why geologists seek rapid, non-destructive spot analysis methods. Here, the capabilities of LIBS are evaluated and compared to those of a portable XRF, which generally fulfills the above-mentioned requirements.

Ammonites were cephalopods occurring from the Devonian to the Late Cretaceous, where they completely disappeared during the well-known mass extinction of the Cretaceous–Tertiary boundary [18]. They are among the most frequently used fossils for building a temporal framework based on organism assemblages (a method called biostratigraphy). Besides their chronological capabilities, ammonites belonged to ecological communities, which are nowadays studied to reconstruct paleoenvironments [19]. Their fossilization process is an important issue for such a purpose. Among the numerous modes of fossilization which may occur, diagenetic pyritization and phosphatization are common. In the phosphatization process, the original aragonite of the ammonite shell is changed into calcium phosphate by replacing carbon with phosphorus. In pyritization, dissolved iron originating from the surrounding sediment precipitates under the form of iron sulfide [20]. Sometimes the shell vanishes and only the internal mold remains. As this later process depends in part on the organic matter content, it may inform about paleoenvironmental conditions. With a portable LIBS, shooting at the same location provides elemental depth profiles, allowing the shell to be chemically distinguished from the internal mold sediment. Its use may help to recognize fossilization processes in the field, and to select specimens suitable for further complementary studies in the laboratory.

2. Experimental

2.1. Portable LIBS system

A pulsed Nd^{3+}:YAG flash lamp laser, emitting at the fundamental wavelength of 1064 nm and actively Q-switched (with double pulse capability), was used as the laser source of the portable LIBS system (see [12] for more details about main characteristics). The energy distributed in one pulse is up to 40 mJ, with a duration time of 4.5 ns and a repetition rate up to 1 Hz. No advantage was recognized in applying a double pulse regime [21,22] for our samples, so that the laser always operated in single pulse mode. As the beam quality M^2 is about 14, a telescope with a magnifying factor of 2 was used in combination with a focusing lens of short focal length of 50 mm. Such an optical arrangement produces a laser spot less than 500 μm (typically 350 μm) in diameter. Two crossed red laser beams, associated with four white LED lighting the sample surface, and a compact color camera, allow the operator to choose the shot position. The plasma light generated by the laser shot is collected with an aspheric lens (from Ocean Optics), directly coupled to a transport fiber. A small chamber is situated between the focus point of the laser and the collecting lens. This chamber is separated from the laser arrangement by a fuse UV-silica plate. Two O-rings are placed between the sample and the chamber, and between the chamber and the silica window. This closed volume allows various gases, pressures and air flows to be used. As a consequence, this configuration notably improves shot-to-shot stability and signal intensity [23]. It also reduces optic contamination by removing dust produced by laser ablation.

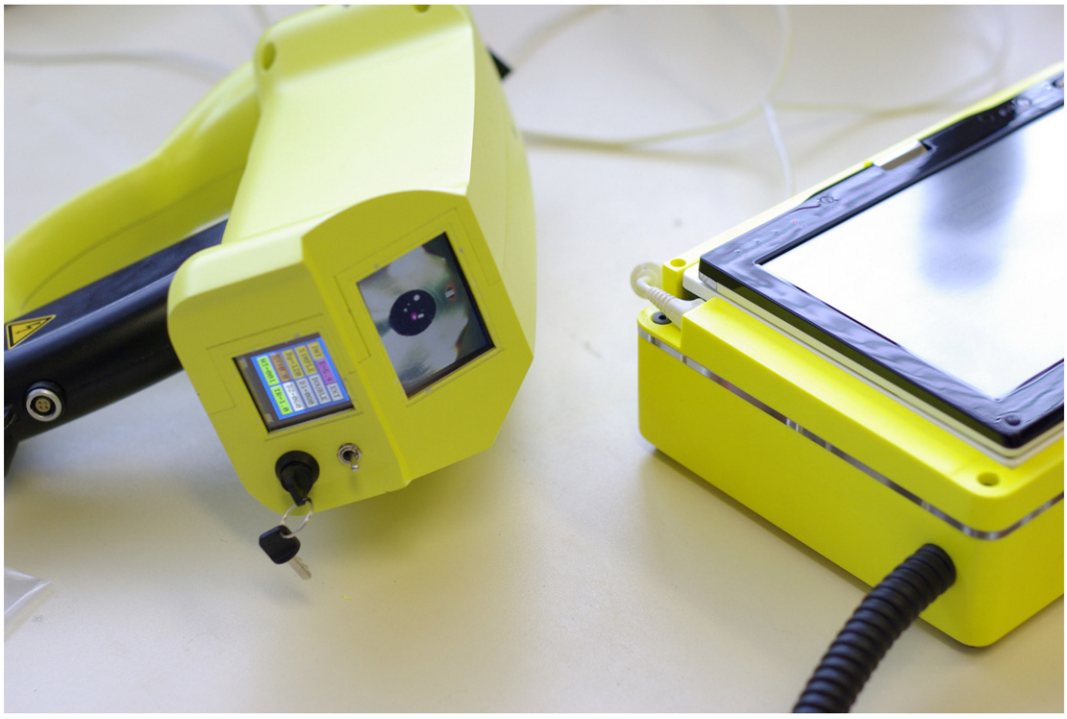

Fig. 1. Portable LIBS system and its two main parts, connected together with the umbilical.

All these optical elements are mounted within a gun-shaped box, designed for comfortable handling (see Fig. 1). Two color screens are installed at the back of the gun. They display the laser settings and the picture from the camera. The "laser gun" is connected by an umbilical to a second box containing the spectrometer, the batteries, a computer, a small pump, and a filter. Inside the umbilical, there is a fiber transmitting light to the spectrometer, space for exhausting the sample chamber, and several wires to power and control the laser. The spectrometer is a small Czerny-Turner Ocean Optics HR 2000+. Its bandwidth ranges from 200 nm to 650 nm in wavelength, with an optical resolution of 0.4 nm (spectral resolution of about 1000). It possesses triggering capabilities with minimal integration time of 1 ms. A single broadband spectrometer with low spectral resolution was preferred to several narrowband spectrometers with high spectral resolution in order to maintain volume, weight and cost as low as possible. Our configuration offers a large spectrum allowing several elements to be measured. The overall control of the system is provided by a small touch screen computer. The software for acquisition and spectra processing was especially developed for this LIBS system. It provides automatic correction of the background, the thermal shift of spectral line positions, and the calibration of the spectrometer. It also possesses an automatic detection mode able to associate spectral lines to their corresponding chemical elements. The system is completely autonomous. Its working time is limited by the computer and the battery lifetime of about 6 h. The total weight of the system is 5 kg.

2.2. Tephra layer

A sampling campaign was undertaken in the deposits of the littoral platform of the lake du Val (Jura, France, 46° 37.917′ N; 5° 48.825′ E). The lake, with a surface area of 64 ha, is known to have received and archived the atmospheric inputs (i.e. tephra layer) resulting from the Laacher See volcano eruption. A 4.35 m sediment sequence, spanning the end of the Late Glacial and the entire Holocene, was recovered using a Russian peat corer (6 cm in diameter and 100 cm in length). The whole core sequence (Fig. 2), reconstructed by overlapping five core segments, highlights five main lithological units as follows, from the base to the top: (unit A) gray laminated clayey silt; (unit B) lacustrine chalk including the black Laacher See tephra layer at 3.67 m depth; (unit C) dark gray clayey silt; (unit D) a thick unit of lacustrine chalk with a dark organic layer at 2.96 m depth; (unit E) organic mire and peat. The core was logged at 5 mm increments with a Bartington MS2 point sensor for high-resolution magnetic susceptibility (MS) measurement. MS values are generally low (less than 10 SI), typical of carbonate deposits. A sharp peak, reaching 156.4 SI at 3.67 m depth, is nonetheless measured within a ~5 mm black layer (Fig. 2). Such intensity at this depth in a lacustrine chalk unit (unit B) corresponds to the well-known volcanic magnetic minerals originating from the LST ash deposit recorded in the Jura Mountains [17]. The sedimentary material presented a high water content (>60%). As a consequence, the laser pulse energy was in great part consumed by water evaporation

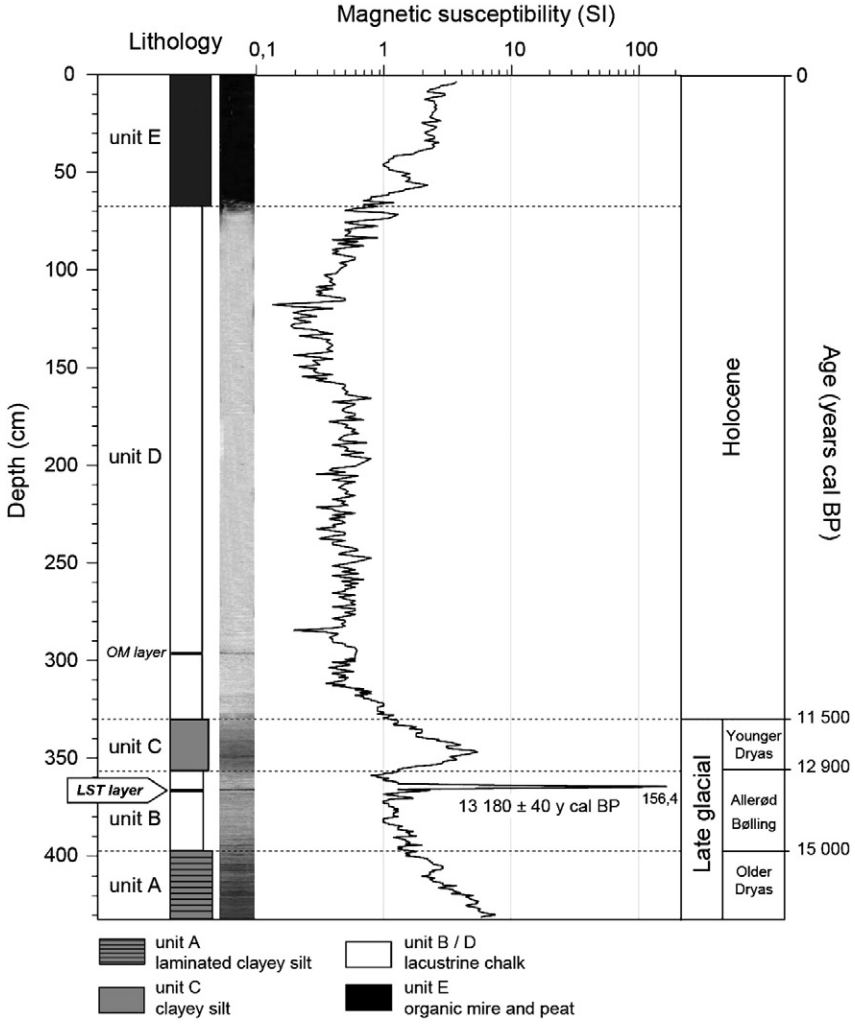

Fig. 2. Lithology, magnetic susceptibilty profile and chronology of the lake du Val core (Jura Mountains). The MS peak corresponds the LST position, at a depth of 3.67 m.

processes [24], so that the spectroscopic signals were too low to provide measurements in humid conditions. The sedimentary sequence containing the LST was then cut into smaller pieces and dried at 50 °C overnight. The drying process is also referenced to improve signal stability in the case of powder samples [25,26]. For the spectra acquisition two different methods were used:

(a) Multiplying shots at a single location, then shifting locations by 1 mm along a line drawn perpendicularly to the tephra layer.
(b) Operating single shots, with locations distributed regularly over the surface in order to create a grid of points 0.5 mm apart perpendicular to the ash layer and 0.25 mm apart parallel to it.

In both cases, the laser was fixed in one position and the sample was moved by an automatic transition system. The system was triggered by a photodiode exposed to plasma emission. The acquired spectra were normalized to the sum of the whole spectrum intensity. The intensity of every selected spectral line for all acquired spectra was automatically integrated and background corrected by the software. The following elements and corresponding spectral lines were chosen: Al I – 396.15 nm, Ca I – 487.81 nm, Fe I – 358.12 nm, Ti – 498.17 nm, Ba II – 455.40 nm and Na I – 589.00 nm. These lines were selected in order to avoid as much as possible interference from other elements. In the case of the Al I – 396.15 nm line, there is however strong interference from the Ca II – 396.85 nm line. Other possible Al lines exist at 308.22 nm and 309.27 nm, but the signal-to-noise ratios are too low in this part of the spectrum. An Fe line also interferes with the selected Ti line. Nonetheless, the lack of correlation between this Ti line intensity and the stronger Fe line suggests that measuring Ti – 498.17 nm does not constitute a major drawback.

For comparison, a commercial portable XRF system – Delta Handheld XRF from Innov-X Systems – was also used. The device, which is originally hand held, was attached to a closed-beam workstation, and was controlled by dedicated software. Elemental quantification was carried out using an implemented 3-beam analysis method (integration time of 30 s for each beam) optimized for the analysis of heavy, transition and light elements in soils. Before the measurements, a calibration process was performed, as suggested by the manufacturer. It consists in a calibration check, blank (pure commercial SiO_2) measurement, and one or several measurements of certified reference materials (CRMs): NIST 2781 and NIST 2702. Acquisition was performed on the sedimentary sequence in different positions, on a line of 50 mm, perpendicular to and centered on the tephra layer, with a step of 2.5 mm. The diameter of the measurement window is about 15 mm. Daily reproducibility was estimated under the basis of the values obtained on the CRM replicates. Relative standard deviations (RSDs%) of 2–10% were computed for lithophilic elements, such as Ti and Fe, while the RSD% of Ba was much higher, at about 35%. This value is a consequence of the high uncertainties related to each measurement, for which individual RSDs% vary between 20 and 40%, at a concentration level for Ba of 400–600 $\mu g.g^{-1}$. In order to obtain a significantly more precise Ba measurement for the Lasher See layer, the acquisition time was multiplied by 3 when approaching the tephra horizon. Certified values, when provided, allowed the accuracy of XRF measurements to be checked. The recovery was 156–181% for Ti and 110–120% for Fe. Such values lead to clear overestimations from a purely quantitative point of view, but as measurements were proved to be fairly reproducible, the examination of XRF-derived profiles should provide good indications of variability in chemical compositions along the sequence.

2.3. Ammonites

The ammonites were collected from the Belmont quarry, located close to Lyon, France. These outcrops are dated from the Lower to Middle Jurassic (Toarcian to Aalenian). The ammonites studied come from the Toarcian stage. One of the main interests of the quarry is that it offers the opportunity to test various modes of fossilization (pyritization and phosphatization). Five different ammonite species were selected.

Specimens A1 and A2. *Dumortieria munda*. They possess well preserved thin ribs, and are completely white. This type of fossilization is generally considered as phosphatization, which may correspond to a chemical transformation of the initial aragonite (calcium carbonate) shell. They belong to the Pseudoradiosa Zone (Lower Jurassic).

Specimens B1 and B2. *Hildoceras bifrons*. They are black or dark red and are supposed to be pyritized on their external parts. They are fossilized as internal molds (absence of external shell layers). They belong to the Bifrons Zone (Lower Jurassic).

Specimen B3. *H. bifrons*. It is grayish green without any visible shell layer. Therefore, the specimen seems to be an internal mold, totally composed of sediments. It belongs, like B1 and B2, to the Bifrons Zone (Lower Jurassic).

Specimen B4. *Hammatoceras* sp. It is grayish red, without any visible shell layer. Therefore, the specimen seems to be an internal mold, totally composed of sediments. It belongs to the Variabilis Zone (Lower Jurassic).

3. Results and discussion

3.1. Spectrometer

The most critical part of a compact LIBS system is the spectrometer, which has to be compact, light, and energy saving. To evaluate the limitation of the Czerny-Turner installed in the LIBS, it was compared with a high spectral resolution (up to 4500) Echelle spectrometer [27,28]. With the Czerny-Turner spectrometer, the Sr II and Fe I lines are difficult or impossible to resolve, while self-absorption is not observable for the Ca I line as self-reversal (Fig. 3). The resolution is low, about 0.4 nm, but sufficient for identification of many lines corresponding to a large number of elements, when interferences between spectral lines are avoided. Such a resolution does not permit a fully quantitative analysis [29–31]. However, interesting conclusions about relative variations of elemental concentrations can be drawn, given that measurements are carried out on material of the same nature in order to prevent matrix effects [32].

As the sensitivity of the CCD detector used in the compact spectrometer is weak in the UV part of the spectrum, whereas the electronic noise is steady, the signal-to-noise ratio decreases greatly at short wavelengths. This noise can be reduced or suppressed by signal accumulation as depicted in Fig. 4. In practice, the number of shots accumulated is however limited by the low repetition rate of the laser (maximum 1 Hz), and by the nature of the samples (see section 3.2.

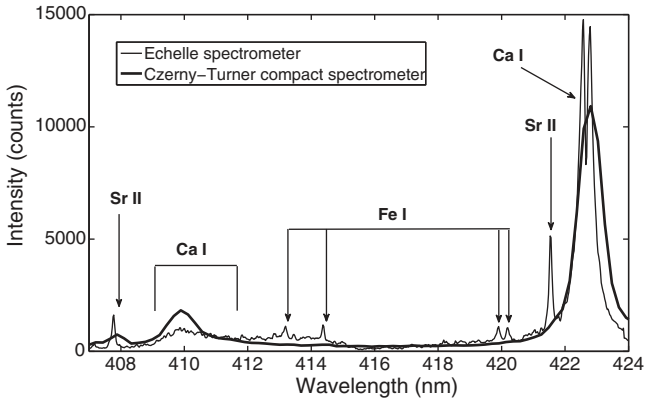

Fig. 3. Comparison of the resolution of a compact Czerny-Turner spectrometer and an Echelle spectrometer under the same analytical conditions. Spectra were acquired from a bentonite sample (a phylosilicate mineral previously analyzed by ICP-MS) in the blue part of the spectrum. Lines of geological interest are indicated.

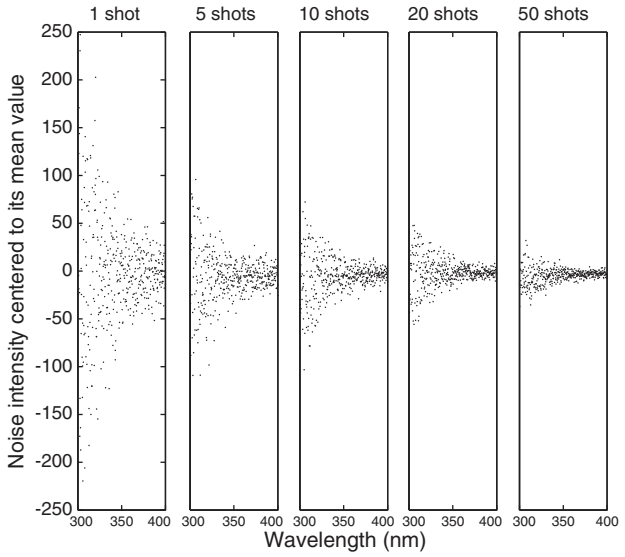

Fig. 4. Noise intensity (centered to the mean value) versus wavelength in the UV part of the spectrum (300–400 nm) for 1, 5, 10, 20 and 50 laser shots accumulated. The input of the Czerny-Turner spectrometer was closed during the acquisition.

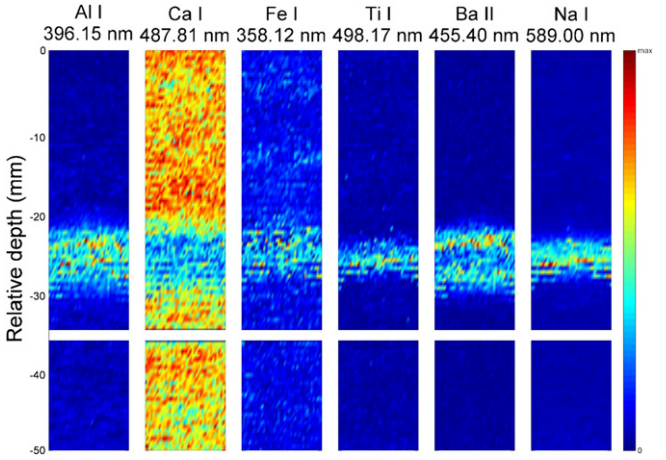

Fig. 6. 2D elemental abundance map for a 50 mm (vertical) × 10 mm (horizontal) part of core centered to the tephra layer. The origin of the Y-axis corresponds to the depth 3.645 m of the original core. The white horizontal bar at ~−35 mm of relative depth corresponds to a 2 mm-wide crack in the core where measurements were not possible. Laser was operated in single shot mode, producing a total of 100 × 40 points. Intensity of lines is depicted by a color code.

below) [33,34]. As a result, the visible lines (400 to 650 nm) are privileged for further processing.

3.2. Tephra layer

Preliminary tests were conducted on lacustrine chalk to optimize acquisition parameters (intensity and signal-to-noise ratio). Fig. 5 exhibits the evolution of signal intensity and RSD% in relation to the number of shots performed at the same location. All line intensities fall to ~30% compared to the first shot, and stabilize after approximately 13 shots. The RSD% can reach more than 50% after 17 shots. After 20 shots the crater reaches approximately 1 mm in diameter and depth. Such a large volume of removed material is due to the specific nature of the sample (a powder), which is easily expelled by the shock wave from plasma expansion. The ablation of material from the focal point is responsible for the degradation in quality of the measurements. Accumulating shots in the same position did not improve signal intensity, signal-to-noise ratio, or RSD%, as initially expected. The best choice consists either in moving the laser spot to different but close locations after each shot (rastering), or in limiting the number of shots. A rastering procedure requires a precise displacement of the system that is hardly compatible with our portable, handheld system.

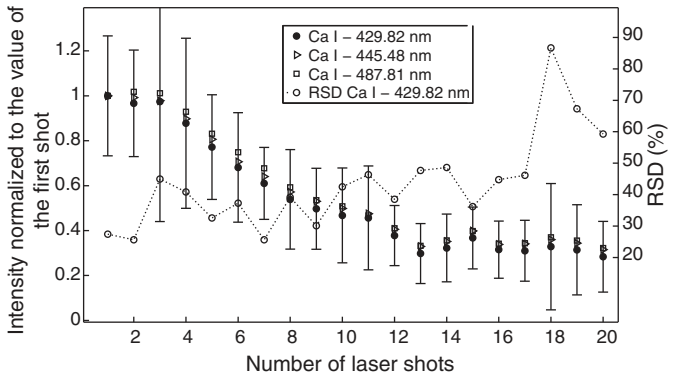

Fig. 5. Intensity (normalized to the value of the first shot) and RSD% vs number of laser shots for three calcium lines. Tests were performed on the lacustrine chalk sample, shooting at the same location (the whole operation was repeated 15 times). Error bars correspond to the standard deviation for the Ca I – 429.82 nm line.

Several 2D elemental abundance maps were produced for a segment containing the tephra layer. The area of interest covers 50 mm (vertical) x 10 mm (horizontal) (Fig. 6). The tephra layer is clearly noticeable by a positive anomaly in Fe, Na and terrigeneous elements (Al, Ti, Ba), which are all strongly and positively correlated, and by a negative Ca anomaly, which can be taken as a surrogate of carbonaceous chalk content. Such behavior is even clearer in a section view performed by averaging all 40 horizontal points of the slice for each vertical position, namely LIBS-40 (Fig. 7). A one-dimensional (vertical) transect was performed as a test along the sedimentary sequence, using only 5 shots, namely LIBS-5 (Fig. 7). With such settings, line intensities should decrease, at most, to approximately 70% of the first shot (Fig. 5), while the measured crater diameter does not exceed 0.3 mm. Using only 5 shots limits the acquisition time, but it is hoped that measurement quality will not be drastically degraded. The Ba, Al, Ti and Na profiles obtained by LIBS-5 are comparable to those computed from the map (LIBS-40), and therefore exploitable to detect the tephra layer. In contrast, Ca and Fe profiles become too noisy to be of real geological interest. XRF-derived Ti, Fe and Ca results are in good agreement with LIBS-40. For Ba, the situation is less clear because several positive anomalies, which are not detected with LIBS-5 and LIBS-40, are measured with XRF. To summarize, the tephra layer is characterized by high Ti, Ba Al, and Na content which can be easily detected by LIBS and by XRF for the first element. However, as the measurement window of the XRF has a diameter of approximately 1.5 cm, the Ti profile obtained by this method is over-smoothed in comparison with those deriving from spot analyses by LIBS. LIBS is able to distinguish two local maxima within the ash layer (which might be the result of post-depositional migration), while XRF measurements provide a single broad peak.

Simulations were performed from the elemental abundance maps to optimize the acquisition settings in the case of handheld measurements. Two circles 5 mm in diameter were selected: one in the middle of the tephra layer and the other within the lacustrine chalk. From 1 to 30 shots, replicated 1000 times, were simulated at random positions in both circles. The resulting mean values, with their 95% confidence intervals, are depicted in Fig. 8. Except for Fe, differences between the tephra layer and the surrounding lacustrine chalk can be determined successfully by only 2 shots, except for Fe I — 404.58 nm; nine shots are necessary to eliminate the overlap of the two 2-sigma error bars.

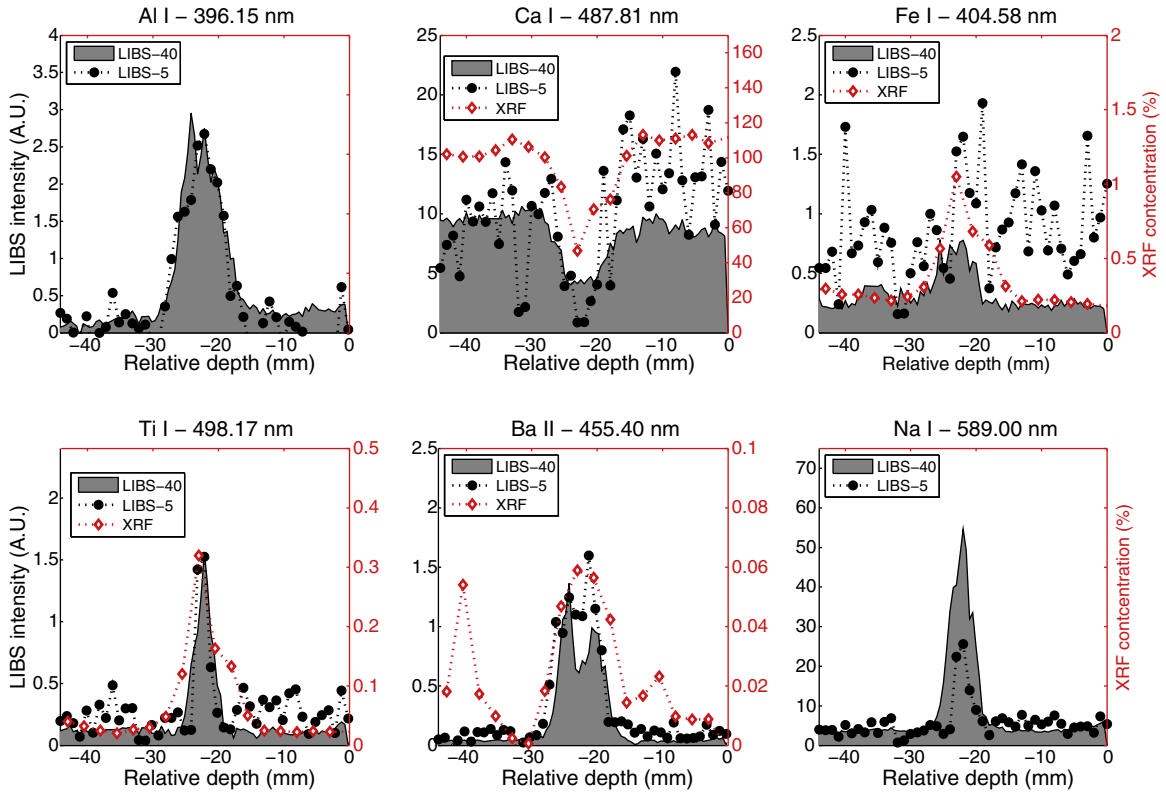

Fig. 7. Line intensities Al, Ca, Fe, Ti, Ba and Na with depth. The origin of the Y-axis corresponds to the depth 3.645 m of the original core. LIBS-40 profiles are computed from the 2D elemental abundance maps (see text), LIBS-5 corresponds to the average of 5 shots from a same location. XRF measurements are provided for comparison. A.U.: arbitraty unit.

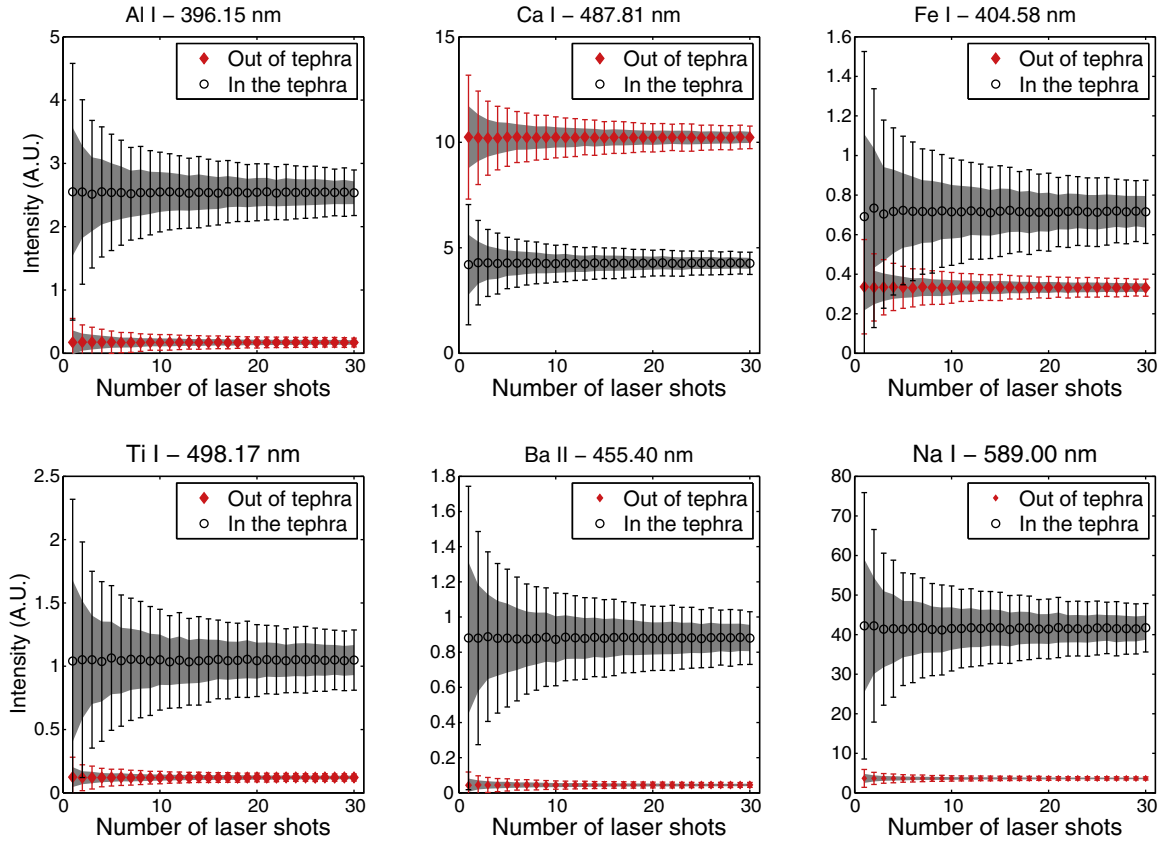

Fig. 8. Mean line intensities, standard deviation (gray area) and 95% confidence interval of the mean in and out of the tephra following the number of simulated shots. For every number of shots, 1000 simulations were generated. A.U.: arbitraty unit.

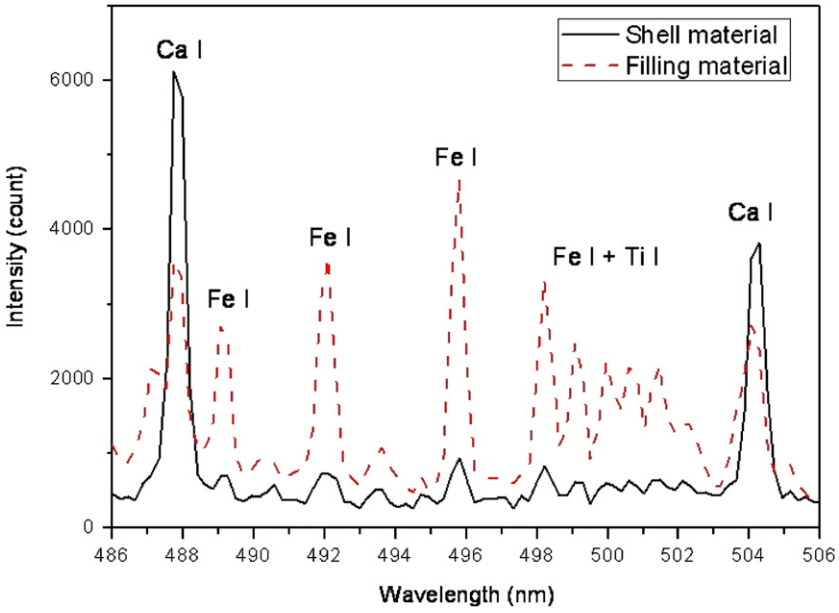

Fig. 9. Intensity spectra of shell and infilling material for the ammonite A1. The spectral lines corresponding to Ca, Ti and Fe are reported.

3.3. Ammonites

Phosphatization processes. The most straightforward approach to study the phosphatization process would consist of monitoring phosphorus content. To test the possibility of phosphorus emission line detection, an InP wafer (for semiconductor industry) was used as a sample. The lines of this element are usually detected at the wavelengths of 253.65 nm, 255.32 nm [35], 213.62 nm, and 214.92 nm, or in deeper UV. As mentioned above, it was not possible to detect any phosphorus line in the 213.62–255.32 nm range with the InP wafer, because of the low signal-to-noise ratio. In the deeper UV part of the spectrum, the lines are also too weak to be detected. The situation did not improve when a greater number of shots was accumulated. As a result, it is not possible to determine the phosphatization process by direct determination using our portable LIBS system. Complementary measurements may however provide useful information. The white ammonites (*D. munda*, A1 and A2), assumed to be phosphatized, were measured by accumulating 10 laser shots at a single location both (i) on the white material constituting the shell, and (ii) on the red material filling the shell. High Ca peaks, more particularly the peak at Ca I – 487.81 nm, are observed in the shell, while the presence of Fe-rich filling material is demonstrated by a notable peak at Fe I – 495.76 nm (Fig. 9). The same behavior can be observed with Al (although not visible in this spectral range) and Ti, which are both only present in the infilling material.

Accumulating shots at the same position is equivalent to digging samples. It can therefore be considered as producing an elemental depth profile in relation to the ablation power of the laser. A total of 275 spectra, performed with 2 shots each, was acquired at the shell surface of the A1 specimen. The Ca I – 422.67 nm/Fe I – 492.05 nm intensity ratio was around 120 for the 130 first spectra, then decreased abruptly to ~20 and remained steady up to the last spectra (Fig. 10). The breaking point around the #130 spectrum clearly illustrates the transition between the shell and the infilling material. As a result, shell and infilling material can easily be distinguished by their chemical signature using LIBS.

Pyritization processes. As with the white ammonites, shell and infilling material of the B1 specimen are chemically different in terms of Ca, Fe and Ti intensity lines (Fig. 11). The situation is however reversed as the shell is enriched in Fe, while the infilling material is Ca-dominated. For the ammonites B1 (B1a and B1b) and B2, suspected

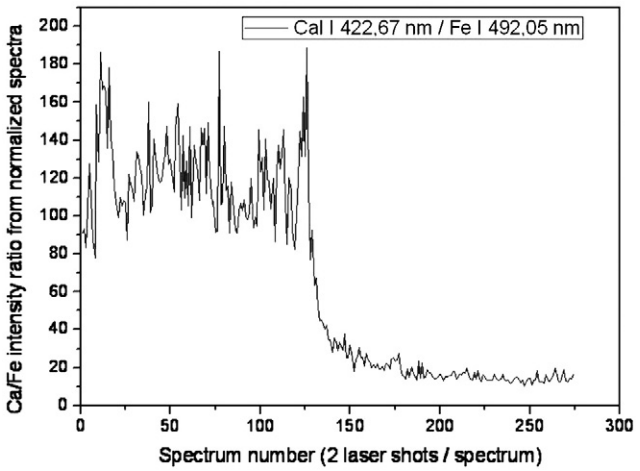

Fig. 10. Ca I – 422.67 nm/Fe I – 492.05 nm line intensities ratio for 275 spectra, all acquired at the same locations on the white A1 ammonite. Intensities are obtained after accumulating two laser shots and normalizing to the total area.

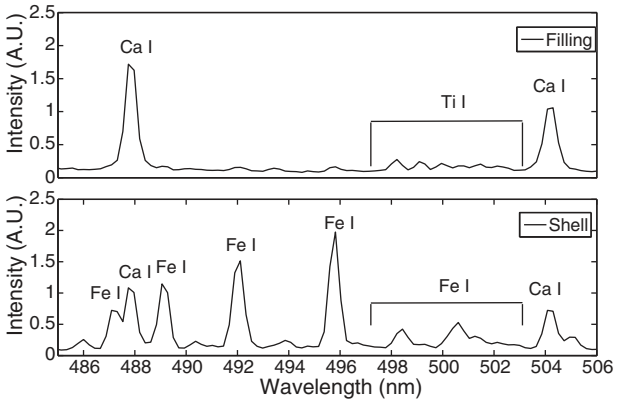

Fig. 11. Intensity spectra of shell and infilling material for the ammonite B1. Each spectrum corresponds to the average of 25 shots. A.U.: arbitraty unit.

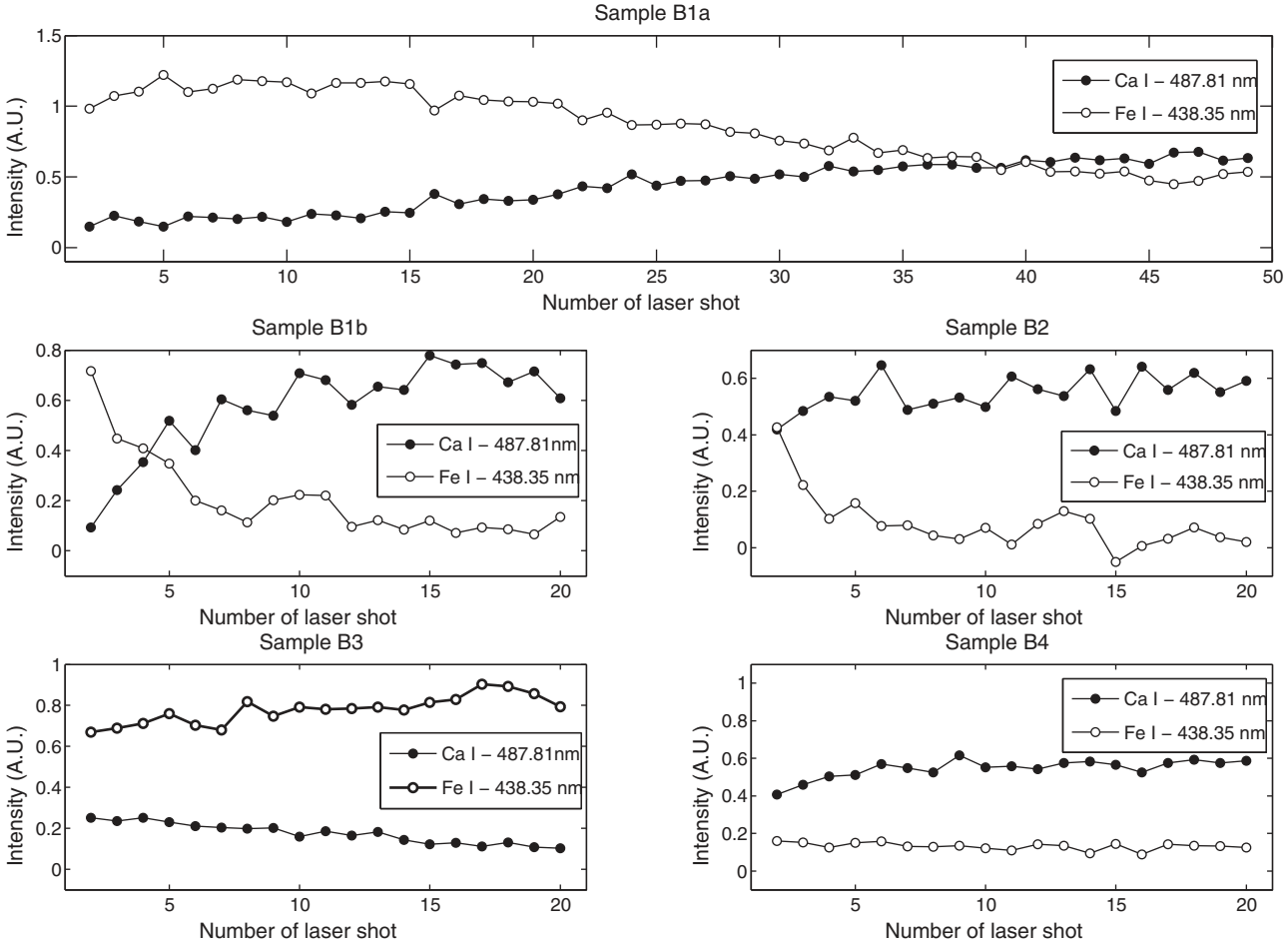

Fig. 12. Intensity evolution of Fe I – 438.35 nm, Ca I – 487.81 nm and Al I – 396.15 nm lines as a function of the number of shots for ammonites B1, B2, B3 and B3. Shots were operated at two different locations for specimen B1 (named B1a and B1b). The first shot was systematically discarded because it was considered as a cleaning shot. A.U.: arbitraty unit.

of pyritization, elemental profiles exhibit similar patterns: Ca line intensities increase with the number of shots, while Fe mirrors the Ca variations (Fig. 12). The negative correlation observed between Ca and Fe is perfectly compatible with the assumption which consists of replacing Ca by Fe during the pyritization process. The Ca and Fe profiles at B1a present however a lower slope. This is related to the greater thickness of the pyritized layer at that location. Line intensities do not drastically change with the number of shots for specimens B3 and B4 (Fig. 12). Such results are chemically in good agreement with our primary visual inspection, which suggested that each fossil was totally composed of homogeneous material, without any shell preservation.

4. Conclusion

To the best of our knowledge, this is the first time that a portable LIBS system has been efficiently used to identify tephra layers in lacustrine chalks. A clear geochemical difference between the tephra layer and lacustrine chalks was observed for Al, Ca, Ti, Ba, and Na. For Fe, the difference becomes clear after 9 shots because the geochemical contrast between ash and the surrounding layers is low. The thickness of the ash layer appears different when assessed with Na and Ti (5 mm) and Al, Ca and Ba (10 mm), probably because of post-depositional migration of the latter group of elements. In any case, the LIBS system provides more accurate thickness determination than XRF because of the large acquisition window in the XRF. Al and Na were not successfully detected by XRF, whereas K, Cr, Mn, Co, Zn, Rb, Sr, and Zr, were determined by XRF, but not detected by the portable LIBS.

The resolution of the spectrometer and the sensitivity in the UV region is not adapted to the study of the phosphatization process. The pyritization process was chemically identified on precisely those 2 ammonite specimens that appeared as black or dark red to the naked eye. An interesting application – because of the spot analysis capacities of the LIBS – would be determining chemical shell patterns of several specimens from the same layer in order to study fossilization processes and their homogeneity.

Our portable LIBS system can therefore already be considered as a useful and practical on-site tool for geology. Semi-quantitative or quantitative measurements, long sought after by geoscientists, could be the next improvement to our portable LIBS.

Acknowledgments

We thank Synerjinov for support in laser part development, as well as the Ministry of Education, Science, Research and Sport of Slovak Republic for the grant VEGA 1/1157/11. We thank the two anonymous reviewers for their constructive comments. We are also grateful to C. Chateau-Smith for help with English.

References

[1] D.W. Hahn, N. Omenetto, Laser-induced breakdown spectroscopy (LIBS), part II: review of instrumental and methodological approaches to material analysis and applications to different fields, Appl. Spectrosc. 66 (2012) 347–419.
[2] R. Neuhauser, B. Ferstl, C. Haisch, U. Panne, R. Niessner, Design of a low cost detection system for LIPS, Rev. Sci. Instrum. 70 (1999) 3519–3522.

[3] D.A. Cremers, M.J. Ferris, M. Davies, Transportable laser-induced breakdown spectroscopy (LIBS) instrument for field-based soil analysis, Proc. SPIE 2835 (1996) 190–200.
[4] K.Y. Yamamoto, D.A. Cremers, M.J. Ferris, L.E. Foster, Detection of metals in the environment using a portable laser-induced breakdown spectroscopy instrument, Appl. Spectrosc. 50 (1996) 222–233.
[5] R.T. Wainner, R.S. Harmon, A.W. Miziolek, K.L. McNesby, P.D. French, Analysis of environmental lead contamination: comparison of LIBS field and laboratory instruments, Spectrochim. Acta Part B 56 (2001) 777–793.
[6] R.S. Harmon, F.C. de Lucia, A.W. Miziolek, K.L. McNesby, R.A. Walters, P.D. French, Laser-induced breakdown spectroscopy (LIBS) — an emerging field-portable sensor technology for real-time, in-situ geochemical and environmental analysis, Geochem. Explor. Environ. Anal. 5 (2005) 21–28.
[7] J. Cuñat, F.J. Fortes, L.M. Cabalín, F. Carrasco, M.D. Simón, J.J. Laserna, Man-portable laser-induced breakdown spectroscopy system for in situ characterization of karstic formations, Appl. Spectrosc. 62 (2008) 1250–1255.
[8] M. Ferretti, G. Cristoforetti, S. Legnaioli, V. Palleschi, A. Salvetti, E. Tognoni, E. Console, P. Palaia, In situ study of the Porticello Bronzes by portable X-ray fluorescence and LIBS, Spectrochim. Acta Part B 62 (2007) 1512–1518.
[9] F. Colao, R. Fantoni, P. Ortiz, M.A. Vazquez, J.M. Martin, R. Ortiz, N. Idris, Quarry identification of historical building materials by means of laser induced breakdown spectroscopy, X-ray fluorescence and chemometric analysis, Spectrochim. Acta Part B 65 (2010) 688–694.
[10] B. Sallé, J.-L. Lacour, P. Mauchien, P. Fichet, S. Maurice, G. Manhès, Comparative study of different methodologies for quantitative rock analysis by laser-induced breakdown spectroscopy in a simulated Martian atmosphere, Spectrochim. Acta Part B 61 (2006) 301–313.
[11] B. Sirven, B. Sallé, P. Mauchien, J.-L. Lacour, S. Maurice, G. Manhès, Feasibility study of rock identification at the surface of Mars by remote LIBS and three chemometric methods, J. Anal. At. Spectrom. 22 (2007) 1471–1480.
[12] J. Goujon, A. Giakoumaki, V. Piñon, O. Musset, D. Anglos, E. Georgiou, J.P. Boquillon, A compact and portable laser-induced breakdown spectroscopy instrument for single and double pulse applications, Spectrochim. Acta Part B 63 (2008) 1091–1096.
[13] P. Bogaard, H.U. Schmincke, Laacher See Tephra: a widespread isochronous late Quaternary tephra layer in central and northern Europe, Geol. Soc. Am. Bull. 96 (1985) 1554–1571.
[14] B. Kromer, M. Friedrich, K.A. Hughen, F. Kaiser, S. Remmele, M. Schaub, S. Talamo, Late glacial ^{14}C ages from a floating, 1382-ring pine chronology, Radiocarbon 46 (2004) 1203–1209.
[15] É. Juviné, S. Kozarski, B. Nowaczyk, The occurrence of Laacher See Tephra in Pomerania, NW Poland, Boreas 24 (1995) 225–231.
[16] G. Bossuet, H. Richard, M. Magny, M. Rossy, Nouvelle occurrence du Laacher See Tephra dans le Jura central. Etang du Lautrey (France), Comptes Rendus de l'Academie des Sciences 325 (1997) 43–48.
[17] A.V. Walter-Simonnet, G. Bossuet, A.L. Develle, C. Bégeot, P. Ruffaldi, M. Magny, T. Adatte, M. Rossy, J.P. Simonnet, J.L. Beaulieu, B. Vannière, M. Thivet, L. Millet, B. Regent, C. Wackenheim, Chronologie et spatialisation des retombées de cendres volcaniques tardiglaciaires dans les massifs des Vosges et du Jura et le Plateau suisse, Quaternaire 19 (2008) 117–132.
[18] In: N.H. Landman, K. Tanabe, R.A. Davis (Eds.), Ammonoid Paleobiology, Plenum Press, New York, 1996, p. 857.
[19] G.E.G. Westermann, New developments in ecology of Jurassic–Cretaceous ammonoids, In: in: G. Pallini, F. Cecca, S. Cresta, M. Santantonio (Eds.), Fossili, Evoluzione, Pergola: Atti del secondo Convegno internazionale. Ambiente, 1990, pp. 459–478.
[20] K.H. Meldahl, 1. Fossilized materials — shells, In: in: D.E.G. Briggs, P.R. Crowther (Eds.), Palaeobiology II, Blackwell Science Ltd, Oxford, 2001, pp. 262–264.
[21] J. Uebbing, J. Brust, W. Sdorra, F. Leis, K. Niemax, Reheating of a laser-produced plasma by a second pulse laser, Appl. Spectrosc. 45 (1991) 1419–1423.
[22] V.I. Babushok, F.C. DeLucia Jr., J.L. Gottfried, C.A. Munson, A.W. Miziolek, Double pulse laser ablation and plasma: laser induced breakdown spectroscopy signal enhancement, Spectrochim. Acta Part B 61 (2006) 999–1014.
[23] A.J. Effenberger Jr., J.R. Scott, Effect of atmospheric conditions on LIBS spectra, Sensors 10 (2010) 4907–4925.
[24] R. Barbini, F. Colao, V. Lazic, R. Fantoni, A. Palucci, M. Angelone, On board LIBS analysis of marine sediments collected during the XVI Italian campaign in Antarctica, Spectrochim. Acta Part B 57 (2002) 1203–1218.
[25] B. Lal, H. Zheng, F.Y. Yueh, J.P. Singh, Parametric study of pellets for elemental analysis with laser-induced breakdown spectroscopy, Appl. Opt. 43 (2004) 2792–2797.
[26] S. Rosenwasser, G. Asimellis, B. Bromley, R. Hazlett, J. Martin, T. Pearce, A. Zigler, Development of a method for automated quantitative analysis of ores using LIBS, Spectrochim. Acta Part B 56 (2001) 707–714.
[27] J.E. Carranza, E. Gibb, B.W. Smith, D.W. Hahn, J.D. Winefordner, Comparison of nonintensified and intensified CCD detectors for laser-induced breakdown spectroscopy, Appl. Opt. 42 (2003) 6016–6021.
[28] B. Sallé, D.A. Cremers, S. Maurice, R.C. Wiens, P. Fichet, Evaluation of a compact spectrograph for in-situ and stand-off laser-induced breakdown spectroscopy analyses of geological samples on Mars missions, Spectrochim. Acta Part B 60 (2005) 805–815.
[29] A. Ismaël, B. Bousquet, K.M. Le Pierrès, G. Travaillé, L. Canioni, S. Roy, In situ semi-quantitative analysis of polluted soils by LIBS, Appl. Spectrosc. 65 (2011) 467–473.
[30] D.L. Death, A.P. Cunningham, L.J. Pollard, Multi-element and mineralogical analysis of mineral ores using laser induced breakdown spectroscopy and chemometric analysis, Spectrochim. Acta Part B 64 (2009) 1048–1058.
[31] J.L. Gottfried, R. Harmon, F.C. De Lucia, A.W. Miziolek, Multivariate analysis of LIBS chemical signatures for geomaterial classification, Spectrochim. Acta Part B 64 (2010) 1009–1019.
[32] J.M. Anzano, M.A. Villoria, A. Ruíz-Medina, R.J. Lasheras, Laser-induced breakdown spectroscopy for quantitative spectrochemical analysis of geological materials: effects of the matrix and simultaneous determination, Anal. Chim. Acta 575 (2006) 230–235.
[33] I.B. Gornushkin, B.W. Smith, G.E. Potts, N. Omenetto, J.D. Winefordner, Some considerations on the correlation between signal and background in LIBS using single shot analysis, Anal. Chem. 71 (1999) 5447–5449.
[34] A.P.M. Michel, Review: applications of single-shot laser-induced breakdown spectroscopy, Spectrochim. Acta Part B 65 (2010) 185–191.
[35] G. Asimellis, A. Giannoudakos, M. Kompits, Phosphate ore beneficiation via determination of phosphorus-to-silica ratios by laser induced breakdown spectroscopy, Spectrochim. Acta Part B 61 (2006) 1253–1259.